Molecular Model of Hemoglobin N from *Mycobacterium tuberculosis* Bound to Lipid Bilayers: A Combined Spectroscopic and Computational Study

Jean-François Rhéault,[‡,§,∥] Ève Gagné,[∥,○,¶] Michel Guertin,[‡,§] Guillaume Lamoureux,[∥,†,⊥] Michèle Auger,[∥,○,¶] and Patrick Lagüe*[,‡,§,∥]

[‡]Department of Biochemistry, Microbiology and Bioinformatics, Université Laval, Québec, Québec, Canada

[§]Institut de biologie intégrative et des systèmes (IBIS), [∥]Regroupement québécois de recherche sur la fonction, la structure et l'ingénierie des protéines (PROTEO), [○]Department of Chemistry, Université Laval, Québec, Québec, Canada

[¶]Centre de recherche sur les matériaux avancés (CERMA), [†]Department of Chemistry and Biochemistry, Concordia University, Montréal, Québec, Canada

[⊥]Centre for Research in Molecular Modeling (CERMM), Concordia University, Montréal, Québec, Canada

Ⓢ *Supporting Information*

ABSTRACT: A singular aspect of the 2-on-2 hemoglobin structures of groups I and II is the presence of tunnels linking the protein surface to the distal heme pocket, supporting the storage and the diffusion of small apolar ligands to/from the buried active site. As the solubility of apolar ligands is greater in biological membranes than in solution, the association of these proteins with biological membranes may improve the efficiency of ligand capture. As very little is known on this subject, we have investigated the interactions between hemoglobin N (HbN), a group I 2-on-2 hemoglobin from the pathogenic *Mycobacterium tuberculosis* (Mtb), and biological membranes using both experimental techniques and MD simulations. HbN has a potent nitric oxide dioxygenase activity (HbN-Fe^{2+}-O$_2$ + •NO + H$_2$O → HbN-Fe^{3+}−OH$_2$ + NO$_3^-$) that is thought to protect

the aerobic respiration of Mtb from inhibition by •NO. Three different membrane compositions were chosen for the studies, representative of the mycobacterial plasma membrane and the mammalian cell membranes. Both the experimental and the modeling results agreed with each other and allow for a detailed molecular description of HbN in association with membranes of different compositions. The results indicated that HbN is a peripheral protein, and the association with the membranes occurred via the pre-A, G, and H helices. In addition, HbN would be allowed to modulate the binding to the membranes via electrostatic interactions between the lipid membranes and the Asp100 residue. In its membrane-bound form the short tunnel of HbN is oriented toward the membrane interior and the other tunnels point toward the solvent. Such protein orientation would facilitate the uptake of nonpolar substrates from the membrane and the release of products to the solvent. It is interesting to note that the pre-A, G, and H helices are conserved among HbN from a few other Mycobacteria.
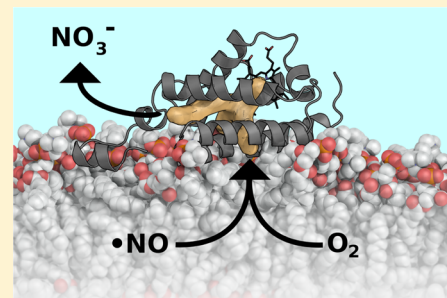
The 2-on-2 hemoglobins (2/2Hbs) are small oxygen-binding hemeproteins present in bacteria, some unicellular eukaryotes, and higher plants.[1−5] Phylogenetic analysis categorized this globin family into three groups, I (HbN), II (HbO), and III (HbP), the proteins being orthologous within each group and paralogous across the groups.[2] On the basis of their biophysical properties, the inferred biological functions of 2/2Hbs comprise nitric oxide (•NO) detoxification[6] and other redox reactions,[7,8] O$_2$ delivery under hypoxic conditions,[9,10] long-term ligand or substrate storage,[1,11] and O$_2$/•NO sensing (for a recent review, see ref 5). Characteristically, the 2/2Hbs are composed of 110−130 amino acids and adopt a 2-on-2 helical sandwich structure, for which the two pairs of α-helices are antiparallel, leading to an α-helical bundle surrounding a buried heme group from the solvent,[3,12,13] as depicted in Figure 1 for HbN from *Mycobacterium tuberculosis* (Mtb).

A singular aspect of 2/2Hbs structures of groups I and II is the presence of cavities organized in branches linking the protein surface to the distal heme pocket (Figure 1), supporting the storage and the diffusion of small apolar ligands to/from the heme. Accordingly, the heme distal site in 2/2Hbs is suited to bind small ligands, likely diatomic gaseous molecules, such as O$_2$, •NO, and CO.[5,13,14] As the solubility of these molecules is greater in biological membranes than in solution,[15−17] the association of group I and II 2/2Hbs with biological membranes may improve the efficiency of ligand capture. For instance, group I Hbs from Mtb,[18] *Chlamydomonas eugametos*[19] and *Nostoc commune*[20] have been localized at the cell
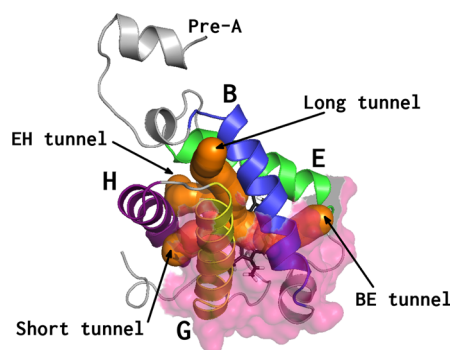
Figure 1. HbN structure (pdb: 1IDR, subunit A). The different tunnels, observed from the crystal structures[13] and MD simulations[11] in solution, are represented by the orange surface. The B, E, G, and H helices are represented by blue, green, yellow, and purple, respectively. The surface highlighted in magenta was predicted to bind to membranes using MPEx[38] (version 3.2.11, using the Wimley-White interfacial scale and a Window length of 19 amino acids). The picture was generated using PyMOL (www.pymol.org).

membrane,[18] while the association of HbO from Mtb with membrane lipids has been demonstrated experimentally.[9,10] Although Hbs are distributed among different cellular compartments (for a review, see ref 21), many other examples of membrane association or localization of Hbs have been reported: *Vitreoscella* Hb,[22−24] the myristoylated Crab globin,[25] the myristoylated or palmitoylated fish GlbX,[26] the avoHb from *Saccharomyces cerevisiae*,[27] the wheat nsHb,[28] the flavoHbs from *Escherichia coli*[29] and *Alcaligenes eutrophus*.[30,31] In a similar case, the binding of the human cytochromes P450 at the membrane interface facilitates the uptake of liposoluble substrates.[32−34] However, no molecular model is yet available for membrane-bound 2/2Hbs that would provide an insight into the molecular mechanism of ligand capture from the membranes. The goal of the present study is to provide such a model and to characterize the interaction between HbN from Mtb and biological membranes.

HbN from the pathogenic bacterium Mtb has a potent ability to detoxify •NO to nitrate (nitric oxide dioxygenase reaction (NOD)) and to protect aerobic respiration from the inhibition by •NO in stationary phase cells of *Mycobacterium bovis* BCG.[6] The high rate of •NO oxidation ($k'_{NOD} \approx 745$ μM^{-1} s^{-1} at 23 °C) catalyzed by oxygenated HbN and the large affinity ($K_d = 8$ nM) for O_2 suggest that the NOD reaction may be one of the vital defense systems in Mtb for coping with the toxic effects of •NO under the low O_2 concentration $(1-4$ $\mu M)$ prevailing in infected lesions.[35] In a previous study, we proposed that this high NOD catalytic activity is related to the efficient capture of •NO by HbN.[36] Effectively, MD simulations of HbN in solution revealed that the entry and the internal diffusion of •NO inside HbN were performed using the long (LT), short (ST), and EH tunnels (Figure 1). However, the ST was preferentially used by •NO to reach the distal heme pocket. This preference is ascribed to its hydrophobic funnel-shape entrance, covering a large area extending far from the tunnel entrance.[36] Although the characterization was done in solution, few insights suggest that HbN might interact with membranes. First, HbN was identified among the lipophilic proteins associated with the cell envelope of virulent Mtb H37Rv.[37] Second, both the membrane protein explorer (MPEx) tool[38] and the positioning of proteins in membranes (PPM) server[39] predict that HbN binds to membranes. The MPEx predicted

HbN segments binding to membranes are presented in Figure 1, while the PPM server prediction of HbN membrane positioning is presented in Figure S1 (Supporting Information).

In this paper, we have investigated the interactions between HbN and membranes using both experimental techniques and MD simulations, for three different membrane compositions: pure DOPC, pure TOCL and a mix of TOCL/DOPE at a molar ratio of 3:1. These lipids were chosen as the CL and PE phospholipids are major structural components of mycobacterial plasma membrane and PC phospholipids are absent from the mycobacterium plasma membranes,[40] but the principal constituent of the extracellular leaflet of mammalian cell membranes.[41] First, the secondary structure of the protein in the presence of membranes was investigated by circular dichroism (CD) spectrocopy. Second, solid-state ^{31}P NMR spectroscopy was used to obtain information on the structure and dynamics of lipid headgroups and thus the effects of HbN on the membrane interface. In addition, Fourier transform infrared (FTIR) spectroscopy was used to characterize the effect of HbN on the hydrocarbon chain conformational order and hydration of the interfacial region. Finally, we have performed MD simulations employing different membrane representations to determine the orientation and the insertion of HbN in the membranes, as well as the dynamics of HbN tunnels when bound to membranes. Both the experimental and the modeling results agreed with each other and allow for a detailed description of HbN in association with membranes of different compositions. The results indicated that HbN is a peripheral protein, and that in its membrane-bound form, the entry of the ST is oriented toward the membrane interior, where the substrates are highly soluble.

■ MATERIALS AND METHODS

Materials. DOPC, DOPE, and TOCL were purchased from Avanti Polar Lipids (Alabaster, AL) and used without further purification. HEPES and EDTA were bought from Fisher (Ottawa, ON) and Sigma-Aldrich (Oakville, ON), respectively. HbN was overexpressed and purified by reconstitution of the apoprotein with heme in a manner similar to the one described previously.[42]

Sample Preparation. The lipid vesicles were prepared by mixing 5 mg of phospholipids in 28.3 μL of a protein solution made in a 100 mM HEPES, 5 mM EDTA buffer at pH 7.5, giving a total proportion of 15% (w/w) of lipids in buffer. The protein concentration was adjusted to obtain a final lipid/protein molar ratio of 60:1. For NMR experiments, the quantity of lipid was scaled up to 12 mg of lipids with the volume of buffer increased accordingly. For CD samples, the protein concentration was fixed at 1 mg/mL, while the quantity of lipid was varied to maintain a 60:1 lipid/protein molar ratio. Then the samples underwent five freeze (liquid N_2)/thaw (41 °C)/vortex cycles. Deuterium oxide (D_2O) was used to eliminate the interference of water in the FTIR spectra, while circular dichroism and ^{31}P NMR samples were prepared using nanopure water.

CD Experiments. CD spectra were recorded with a Jasco J-815 (Easton, MD) circular dichroism spectrometer (Easton, MD). Twenty microliters of the sample was deposited on a quartz cell (Hellma Analytics, Müllheim, Germany) with a 0.01 cm optical path and then inserted into the spectrometer. The spectra were analyzed with Spectra Manager, and the data were thereafter treated using CD-Pro Analysis with the CDSSTR program and the SP37 data set.

NMR Experiments. The ^{31}P NMR spectra were acquired on a Bruker Avance 400 spectrometer (Bruker Biospin, Milton, ON). The sample was placed into a 4 mm NMR tube and inserted into the probe. The spectra were obtained at 161.9 MHz using a phase-cycled Hahn echo pulse sequence with gated broadband proton decoupling.[43] 4 K data points were recorded and 2000 scans were acquired with a 90° pulse length of 4.5 μs, an interpulse delay of 30 μs, and a recycle delay of 4 s. A line broadening of 50 Hz was applied to all spectra. The chemical shifts were referenced relative to external H_3PO_4 85% (0 ppm).

FTIR Experiments. Infrared spectra were recorded with a Nicolet Magna 560 Fourier transform spectrometer (Thermo-Nicolet, Madison, WI) equipped with a narrow band mercury−cadmium-telluride (MCT) detector and a germanium-coated KBr beam splitter. Twenty microliters of the sample were placed between CaF_2 windows sealed with a paraffin solution to prevent ^2H−H exchanges. A total of 128 interferograms were acquired with a resolution of 2 cm^{-1} in the spectral range of 4000−650 cm^{-1} at various temperatures ranging from 12 to 70 °C and controlled by a Peltier device. The spectra were corrected for the water vapor and CaF_2 contribution by subtraction of a reference spectrum. The data were processed with the software Grams 386 (Galactic Industries Corporation, Salem, MA) version 3.03. Both the spectral regions corresponding to the C−H and ester carbonyl stretching vibrations were baseline-corrected using a cubic function. The methylene and ester carbonyl symmetric stretching frequencies were obtained from the center of gravity calculated at the top 10% of the band.

Simulation Details and Parameters. All the simulations were performed with the NAMD molecular dynamic software,[44] unless otherwise noted, using the CHARMM22[45] force field for proteins with the CMAP correction[46] and the CHARMM36[47] parameters for lipids, TIP3P waters,[48,49] a time step of 2 fs, and periodic boundary conditions. Cutoffs for the short-range electrostatics and the Lennard−Jones interactions were 12 Å, with the latter smoothed via a switching function over the range of 10−12 Å. Nonbonded pair lists were updated every 10 steps. Long-range electrostatics were calculated via the particle mesh Ewald (PME) method,[50,51] using a sixth-order interpolation and a grid spacing of ∼1 Å. Drifting of the center of mass due to PME was removed. NPAT ensembles were generated for the biphasic and the highly mobile membrane mimetic (HMMM) systems (see below for details), and NPT ensembles for the bilayer systems and for HbN in solution. Langevin damping with a coefficient of 1 ps^{-1} was used to maintain a constant temperature of 37 °C. The systems were coupled to a Nosé−Hoover Langevin piston to maintain a constant 1 atm pressure. The length of bonds between hydrogens and heavy atoms were constrained using SETTLE for bonds in water molecules, and SHAKE/RATTLE for all other bonds. No other constraint was applied to the systems, e.g., protein binding to membrane observed in simulations did not require the use of external forces or biasing potentials. Coordinates were saved every 5 ps for analysis.

Initial HbN Structure Preparation and Simulations in Solution. Coordinates for MD simulations were taken from the crystal structure of wild-type oxy-HbN (PDB entry 1IDR).[13] All ionizable residues were considered in their standard protonation state at pH 7 with neutral histidine protons placed at the ND1 or NE2 position according to the interactions with their respective neighbors from the crystal

structure. The N-terminal GLYP and C-terminal NTER patches were used for capping. Missing coordinates of the first N-terminal residue and the eight C-terminal residues were built using the internal coordinates definition provided with the CHARMM topology file. The carboxy terminal missing coordinates were optimized by performing 3 ns of Langevin dynamics using CHARMM,[52] with a 1 fs time step and a damping coefficient of 5 ps^{-1}, while keeping constrained all coordinates from the crystal structure. The structure was then immersed in an orthogonal box of water with a 15 Å padding and neutralized with six sodium ions using the SOLVATE and IONIZE plugins from VMD.[53] The system was minimized for 2000 steps and equilibrated by 10 ns of MD simulations using NAMD.[44] The final protein coordinates were used to build the membrane systems, while the whole system was used to perform three 150 ns trajectories of HbN in aqueous solvent to characterize the structure and dynamics of the protein in a membrane-free environment.

Biphasic Solvent Simulations. Biphasic solvent systems[54] were used to determine the orientation of HbN relative to the membranes. The organic phase was composed of 3682 molecules of 1,1-dichloroethane (DCLE) randomly positioned in a box of 120 Å by 120 Å by 35 Å, giving the experimental density for this solvent. The internal coordinate definition and parameters of CGENFF[55,56] were used. This system was minimized and equilibrated for 10 ns using CHARMM.[52] The equilibrated organic phase was hydrated by the addition of a 20 Å layer of pre-equilibrated water molecules on each side. The resulting system was minimized and equilibrated for another 5 ns of MD simulations using CHARMM.[52] The protein structure previousky generated was then positioned at ∼4 Å above the DCLE−water interface, and oriented to expose the hydrophobic segment predicted by MPEx[38] to the organic phase. Four more starting orientations were obtained by rotating the protein around its main vector by 30 and 60° clockwise and counterclockwise. A sixth position was chosen to expose the hydrophobic surface identified by MPEx to the solvent. These initial orientations, referred hereafter as DCLE-1 to DCLE-6, are presented in Figure S2, Supporting Information. The systems were then simulated for 30 ns, with the protein fixed for the first nanosecond. The trajectory frames between 10 ns and the first entering of a DCLE molecule inside the tunnels (the introduction of one or more DCLE molecule(s) into the protein matrix leads to a marked increase in the root-mean-square deviation (RMSD) of the backbone atoms) were used to calculate the average HbN orientation and insertion. As different starting orientations were used for the simulations, not all trajectories were expected to reach an equilibrium orientation and/or insertion. The trajectories that displayed a significant difference (more than 3 standard deviations from the mean) in orientation or insertion were considered as outliers and discarded from analysis.

Highly Mobile Membrane-Mimetic Simulations. The influence of the lipid polar headgroups on HbN binding to membranes was studied using the HMMM[57] lipid representation. Briefly, the membrane hydrophobic core is represented by an organic solvent layer, while the headgroup region is composed of short-tailed phospholipids. This membrane representation accelerates lipid lateral diffusion without sacrificing the atomic details. The topology of three short-tailed lipids were derived from the phospholipid topologies described in the CHARMM36 all atom additive residue

topology file for lipids.[47] The lipids used for the HMMM systems in the present study were divalerylphosphatidylcholine (DVPC), tetravaleryl cardiolipin (TVCL), and divalerylphosphatidylethanolamine (DVPE), derived from the dioleoylphosphatidylcholine (DOPC), tetraoleoyl cardiolipin (TOCL), and dioleoylphosphatidylethanolamine (DOPE), respectively. The HMMM systems were built according to the methodology described in Ohkubo et al.,[57] with the exception that TVCL concentrations were halved. The equilibrated water−DCLE system, from the previous section, was used to build the HMMM systems. Three different membrane compositions were built: pure DVPC, pure TVCL, and TVCL/DVPE at a molar ratio of 3:1 (hereafter referred to as DVPC, TVCL and TVCL/DVPE systems). Three trajectories were produced for each lipid composition, each having a different initial distance between HbN and the interface, defined as the average position of the lipid phosphate groups. The distances were 2, 4, and 6 Å between HbN center of mass and the HMMM interface. The initial orientation was slightly different than the average orientation calculated from the converged water−DCLE trajectories to further expose the HbN surface predicted by MPEx[38] to membranes, giving a membrane tilt angle of 40° for the heme. The systems were then simulated for 50 ns, with the protein fixed for the first nanosecond. Trajectory frames between 10 ns and the first entering of a DCLE molecule inside the tunnels were used to calculate the average HbN orientation and insertion. The trajectories that displayed a significant difference (more than 3 standard deviations from the mean) in orientation or insertion were considered as outliers and discarded from analysis.

Lipid Bilayer Simulations. The equilibrium positions and orientations of HbN from the HMMM simulations were used to build the systems using the classical lipid representations. Three membrane compositions were built: pure DOPC, pure TOCL, and TOCL/DOPE (3:1) (hereafter referred to as DOPC, TOCL and TOCL/DOPE systems, respectively). The bilayer systems were built using modified CHARMM-GUI[58−60] scripts. First, the cardiolipin topology, obtained from the laboratory of Dr. Wonpil Im (personal communication), was included into the scripts. Second, the position of the spheres along the Z axis, in the layer containing the protein, was set to 20 Å instead of 12 Å in the lipid packing procedure. This modification prevented any spheres from being placed under the protein while at the interface, which could result in steric clashes with the lipids molecules. The bilayers were approximately 90 Å by 90 Å in the XY plane, and water molecules were added using a padding of 15 Å along the Z axis between any atom of the protein and the lipids and the sides of the simulation box. The lipid area used to build the membranes were 67.4 Å^2 for DOPC,[61] 124 Å^2[62] for TOCL, and 65 Å^2 for DOPE.[63] The final systems comprised approximately 82 700 atoms, 69 500 atoms and 67 800 atoms for the DOPC, TOCL, and TOCL/DOPE systems, respectively. Three 250 ns trajectories were performed for each lipid composition, each having the same HbN initial position. The protein was fixed for the first nanosecond, and the first 100 ns were considered as equilibration, leaving the last 150 ns for analysis.

MD Simulation Analysis. The tilt angle between the heme plane, defined by the heme nitrogens, and the lipid bilayer normal, defined as the Z axis, was calculated to represent the orientation of HbN relative to the membrane. The most representative configurations, presented in Figures 5 and 6, were defined as the configurations for which the insertion and

orientation of HbN relative to the membrane were the closest to the average values calculated from the trajectories. The relative time of contact between HbN residues and the lipid polar heads, and between the HbN residues and the lipid aliphatic chains were considered. The relative time of contact was defined as the fraction of snapshots from the trajectories in which a contact between any atom from a residue of HbN was in contact with at least one atom of one of the lipid chemical groups. The polar head atoms were defined as any heavy atoms from the phosphatidylcholine, diphosphatidylglycerol, or phosphatidylethanolamine groups from the DOPC, TOCL, and DOPE lipids, respectively. The atoms of the lipid aliphatic chains comprised the carbons from the second position of the acyl chain and beyond. Finally, CAVER 3.0[64] was used to characterize the tunnels of HbN in solution and in the presence of a bilayer. The starting point of the probe was set 4 Å above the heme iron on the distal side, and all the default parameters were used. The tunnel formation frequency was defined as the percentage of snapshots from the trajectories in which a pathway with a bottleneck radius ≥0.9 Å was identified.

■ RESULTS

Circular Dichroism. We have first investigated the secondary structure of HbN in solution and in the presence of the DOPC, TOCL, and TOCL/DOPE 3:1 membrane systems. The CD spectra shown in Figure 2 are very similar for
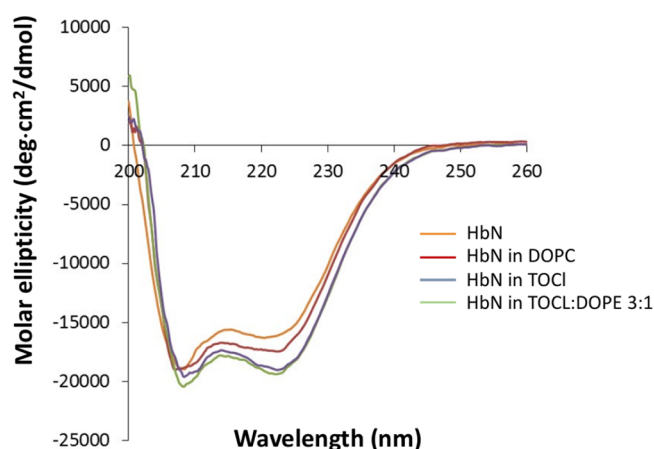

Figure 2. CD spectra of pure HbN and of HbN in DOPC, TOCL, and TOCL/DOPE 3:1 membrane systems. The spectra were recorded at 37 °C.

the protein in solution and in the presence of membranes and reveal a high proportion of α-helices that can be deduced by the presence of two minima at 208 and 220 nm.[65] These results therefore indicate that the secondary structure of the protein is not significantly affected by the presence of membranes.

NMR Spectroscopy. Because of its 100% natural isotopic abundance and its spin of 1/2, phosphorus-31 is the nucleus of choice to study the perturbations induced by proteins in interaction with phospholipids.[66−68] Indeed, the dominant interaction is the chemical shift anisotropy (CSA) which is sensitive to the dynamical and/or orientational changes of the polar head groups. Studying this nucleus can thus give information on the phase and the morphological structures of the phospholipid vesicles.

The results presented in Figure 3 indicate an effect of HbN on DOPC membranes. More specifically, the presence of a
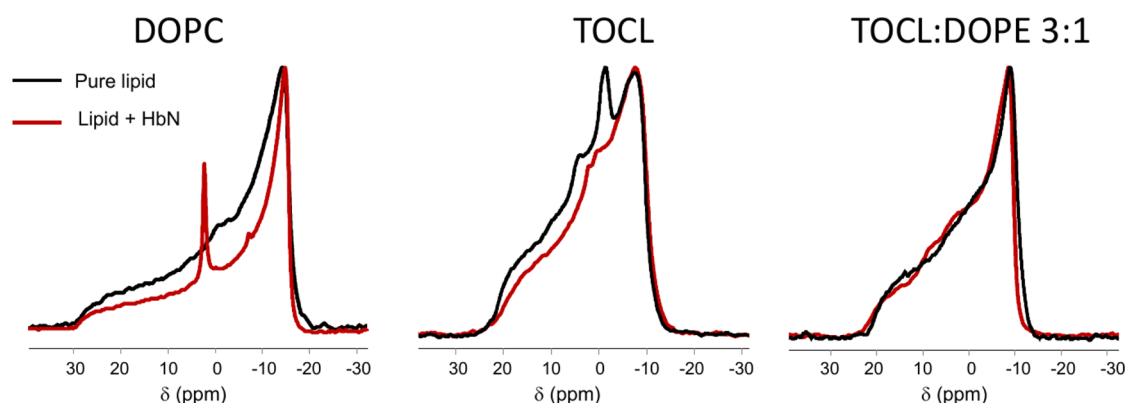
Figure 3. ^{31}P solid-state NMR spectra of pure lipid systems (black lines) and of lipids in the presence of HbN (red lines) at 37 °C.
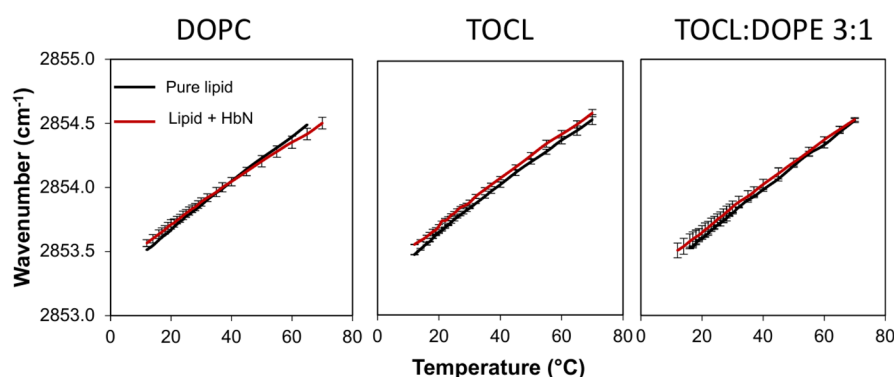

Figure 4. Wavenumber of the methylene symmetric stretching vibration as a function of temperature for pure lipid systems (black lines) and for lipids in the presence of HbN (red lines).

peak at about 3.5 ppm associated with an inverse powder pattern suggests the presence of a small proportion of hexagonal II phase, in addition to multilamellar vesicles in the sample. Micelle formation would have resulted in an isotropic peak at a chemical shift of about −0.5 ppm in the lipid system.[69] This suggests that part of the DOPC lipids experienced a negative curvature in the presence of HbN, possibly due to a deeper penetration of the protein in this lipid system.

Different results were obtained with TOCL bilayers. First, we observed that the TOCL multilamellar vesicles were more spherical compared to the DOPC vesicles which were elongated parallel to the magnetic field, as revealed by the shape of the ^{31}P NMR spectrum.[70] Also, while the spectrum of pure TOCL presented a small isotropic peak at −1 ppm indicating the presence of a small proportion of micelles, this peak was absent in the presence of HbN. This indicates that the protein interacted with the lipid to stabilize the structure and prevent the formation of micelles. For the mixed TOCL/DOPE 3:1 system, the spectra were very similar in the absence and presence of HbN, and the shape of the ^{31}P NMR spectra indicate stable spherical vesicles. This indicates that HbN did not significantly perturbed the morphology of TOCL/DOPE vesicles.

Infrared Spectroscopy. We have used FTIR spectroscopy to investigate the effect of HbN on the lipids by the analysis of the CH$_2$ and C=O stretching vibrations.[71] More specifically, the study of the CH$_2$ symmetric stretching vibration (at about 2850 cm^{-1}), which is sensitive to trans/gauche isomerization in the lipid acyl chains, can provide valuable information about the order of the acyl chains.[71] The thermotropism curves presented

in Figure 4 indicate that HbN had very little effect on the order of the lipid acyl chains for the three lipid systems investigated.

On the other hand, the analysis of the carbonyl stretching vibrations in FTIR spectra can provide information about the effect of proteins on the lipid interfacial region. The C=O stretching vibration, centered at about 1733 cm^{-1}, is the superposition of two bands, one centered at 1740 cm^{-1} and the second at 1727 cm^{-1}.[72] These two contributions correspond respectively to free and hydrogen-bonded carbonyl groups.[73] The C=O stretching vibration is therefore sensitive to the hydration of the lipid interfacial region.

We have investigated the effect of HbN on the hydration of the lipid interfacial region by monitoring the wavenumber of the C=O stretching vibration, and the results are reported in Table 1 at 37 °C for the different lipid systems in the absence and in the presence of the protein. The results indicate a significant increase in wavenumber in the presence of HbN for

Table 1. Wavenumber of the Lipid C=O Stretching Vibration at 37 °C for Different Lipid Systems in the Absence and Presence of HbN[a]

system	wavenumber, C=O vibration (cm^{-1})
DOPC	1732.1
DOPC + HbN	1732.7
TOCL	1733.5
TOCL + HbN	1733.4
TOCL/DOPE	1734.0
TOCL/DOPE + HbN	1734.0

[a]The error is estimated to be ±0.1 cm^{-1}.

the DOPC system, while no significant changes were observed for the TOCL and TOCL/DOPE 3:1 systems. The infrared spectra and second derivative spectra of these different systems are also reported in Figure S3. These results clearly indicate that the presence of HbN increases the amount of free C=O groups in the DOPC lipid system but has no significant effect on the C=O groups of the two other lipid systems.

Overall, these results indicate that the hydration of DOPC bilayers was decreased in the presence of HbN, most likely due to the deeper penetration of the protein in the bilayers which would decrease the formation of hydrogen bonds between the lipid carbonyl groups and the surrounding water molecules.

HbN Binding to Membranes from Simulations. The water−DCLE interface was first investigated using six different protein orientations initially placed 4 Å above the interface (DCLE-1 to DCLE-6, Figure S2, Supporting Information). A stable binding of HbN to the DCLE phase, i.e., a binding of HbN that display no sudden or extreme fluctuations in orientation and insertion, was observed within 20 ns of MD simulations for four trajectories, as depicted from the final snapshots from the trajectories (Figure S4, DCLE-1 and DCLE-4 to DCLE-6), and as indicated by the HbN center of mass and orientation time series (Figures S5 and S6, respectively). From these trajectories, the average center of mass of HbN was located 7.6 ± 0.4 Å above the interface, and HbN was oriented 19.5 ± 2.6° relative to the normal of the interface. The most representative protein orientation and insertion into the DCLE phase is given in Figure 5. The pre-A,
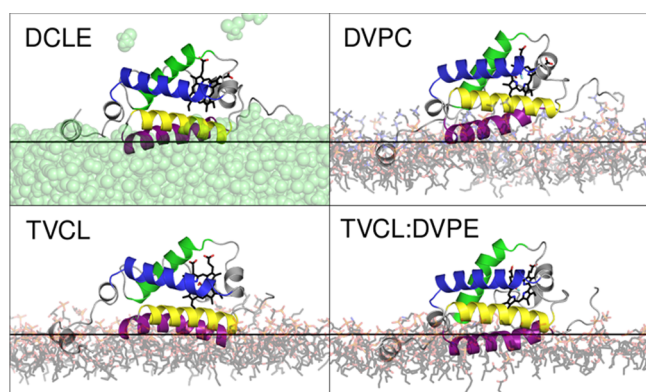

Figure 5. Most representative configurations of HbN bound to the biphasic system and mimetic membranes: the water−DCLE interface (DCLE), the DVPC−DCLE−water interface (DVPC), the TVCL−DCLE−water interface (TVCL), and the TVCL−DVPE (3:1)−DCLE−water interface (TVCL/DVPE). The B, E, G, and H helices are represented by blue, green, yellow, and purple, respectively. Same color code as for Figure 1. The water molecules are omitted for clarity, as well as the DCLE molecules in the presence of the short-tail lipids.

G, and H helices were positioned at the water−DCLE interface, leading to the HbN main axis parallel to the interface. For the two remaining trajectories (DCLE-2 and DCLE-3, Figure S4), HbN diffused away from the interface (DCLE-2) or was located at the interface in a different orientation (DCLE-3), with only a few residues anchoring to the DCLE phase. In all cases, HbN secondary structure remained conserved and stable, as noted by the time evolution of the RMSD (Figure S7) and did not experience any conformational change other than the reorientation of the pre-A helix relative to the rest of the protein (as detailed later). Singularly, the higher RMSD values

observed for DCLE-5 (Figure S7) correlated with the introduction of few DCLE molecules into the protein via the tunnels.

The HbN membrane positioning was further investigated using the HMMM lipid representation for three truncated lipid compositions: DVPC, TVCL and TVCL/DVPE (3:1). Three trajectories were realized for each lipid composition, each having a different initial distance between HbN and the interface. A stable binding of HbN to the membranes was observed within 10−20 ns for all trajectories, depending on the bilayer composition, as noted by the HbN center of mass and orientation time series (Figures S8 and S9, respectively). The binding to the membranes leads to similar positionings between the trajectories for a given membrane composition, with one exception for DVPC-2 for which only the pre-A helix bound to the membrane and the rest of the protein remained in the water phase. The most representative HbN positioning at the interface is presented in Figure 5 for the three membrane compositions. As for the water−DCLE systems, the G and H helices as well as the pre-A segment adopted a horizontal orientation at the membrane interface. In addition, the insertion of HbN into the membranes (∼ 8 Å above the average phosphate group position) and the orientation of HbN relative to the membrane plane (∼25°) were similar for all the trajectories, except DVPC-2, which displayed a different behavior. The RMSD time series, presented in Figure S10, were not stabilized and slowly increased throughout the trajectories. However, HbN secondary structure remained conserved and stable, and the RMSD increases originated from the introduction of multiple DCLE molecules into the protein via the tunnels.

Finally, the HMMM equilibrium positions and orientations were used to build the systems using the classical lipid representations, for three membrane compositions: pure DOPC, pure TOCL and TOCL/DOPE (3:1). Three replicas were performed for each lipid composition, each having the same HbN initial position. As exposed from the HbN center of mass and orientation time series (Figures S11 and S12), the equilibrium protein insertions and orientations were obtained after 150 ns of simulations, which is more than seven times longer than for the HMMM models. The center of mass of HbN stabilized within the first 50 ns of the simulations, for the three membrane compositions, but the protein orientation still fluctuated after 100 ns. The equilibrium values for HbN center of mass and orientation relative to the lipids were similar to what was observed for the HMMM systems, for the three membrane compositions. The most representative HbN positioning at the interface is given in Figure 6 for the three
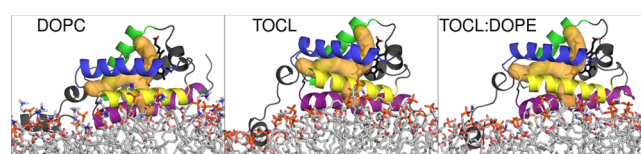

Figure 6. Most representative configurations of HbN bound to bilayers composed of DOPC (left), TOCL (middle), and TOCL/DOPE (3:1) (right). The B, E, G, and H helices are represented by blue, green, yellow, and purple, respectively. Lipids are represented by sticks (carbons in light gray, nitrogen in blue, oxygen in red, and phosphate in orange). The tunnels are indicated by the orange surface. Same color code as for Figure 1. The water molecules are omitted for clarity.
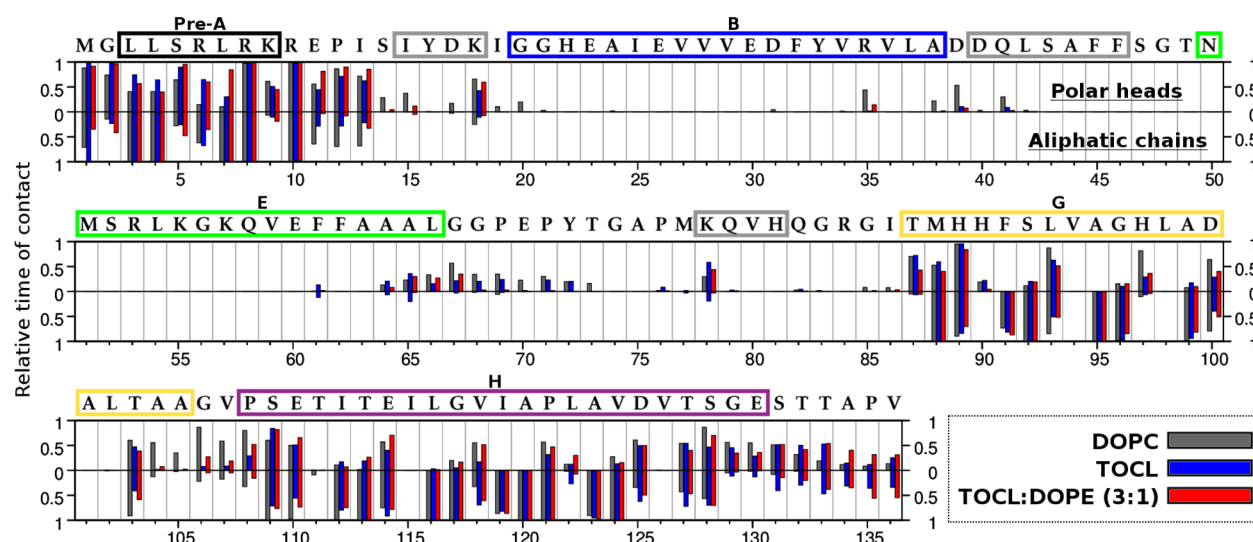
Figure 7. Relative times of contact between HbN residues and lipid polar heads (top halves) and aliphatic chains (bottom halves), for the three membrane compositions (classical lipid representations). Lipids located within 4 Å of protein residues were used for the calculations. The colors of the boxed residues correspond to the helix color code presented in Figure 1, while the gray boxes correspond to the structured loops between the helices.
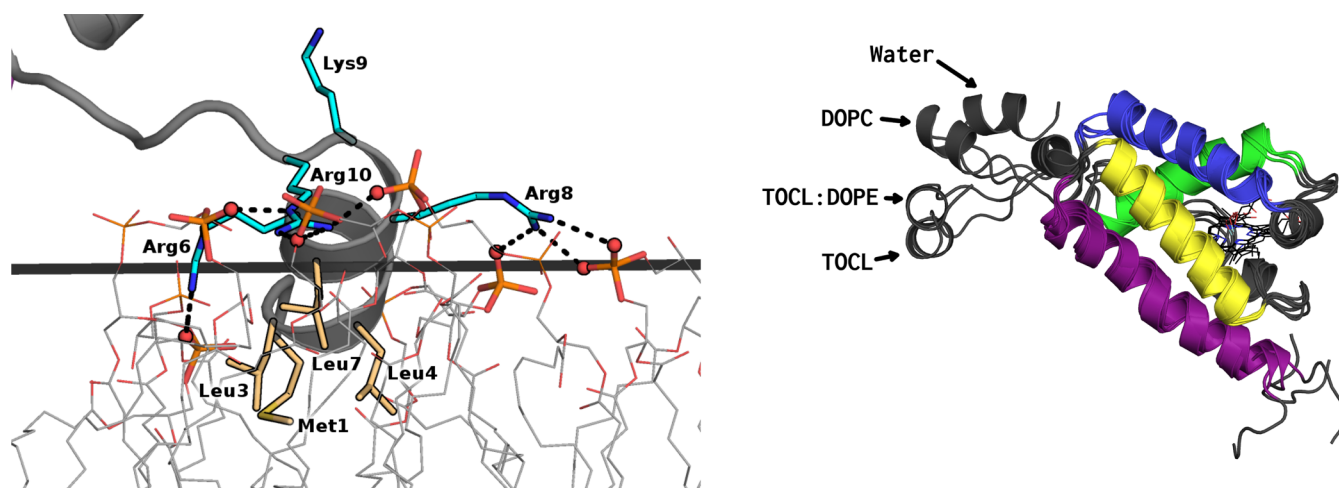

Figure 8. A typical positioning of the pre-A helix at the membrane interface (left), and the reorientation of the pre-A helix relative to the rest of HbN, for the three membrane compositions (classical lipid representations). The black line represents the average lipid phosphate group position along the bilayer normal, the three arginine residues of the pre-A helix are represented in blue sticks, while the hydrophobic residues are in yellow sticks and the lipid phosphate groups in orange sticks.

membrane compositions. These values were 13.1 ± 0.3 Å and 12.7 ± 0.4 Å for the center of mass of HbN in TOCL and TOCL/DOPE bilayers, respectively, compared to 10.4 ± 0.3 Å for the center of mass of HbN in DOPC bilayers. As observed from NMR and infrared spectrocopy, HbN penetrated deeper into DOPC bilayers than other membrane compositions. The center of mass of the pre-A helix, which is the most inserted segment of HbN into the bilayers, were located at a similar depth along the normal of the bilayer for the three bilayer compositions: 0.5 ± 0.2 Å, 0.6 ± 0.2 Å, and 0.5 ± 0.4 Å deeper than the average lipid phosphate level for DOPC, TOCL, and TOCL/DOPE bilayers, respectively. The orientations of HbN relative to the membrane plane were slightly different in the presence of TOCL, 30.9 ± 1.3° and 28.8 ± 2.0° for TOCL and TOCL/DOPE, respectively, compared to 17.7 ± 1.6° for DOPC. Finally, the RMSDs remained under 2.0 Å for all lipid compositions (Figure S13). The secondary structure of HbN in

bilayers remained conserved throughout the simulations (Figure S14).

Time of Contact between HbN Residues and the Lipids. The relative times of contact between the HbN residues and the lipids (classical representation) are reported in Figure 7 for the three membrane compositions. The values are reported for the times of contact with the lipid polar heads and the lipid aliphatic chains. The results from Figure 7 indicate that HbN interacted with the bilayers mainly through the residues of the pre-A, G, and H helices, and the C-terminus, for the three membrane compositions. Notably, the first 13 residues from the N-terminus, which include the pre-A helix, all interacted with both the lipid polar heads and the aliphatic chains, with residues Arg8 and Arg10 in contact with both lipid segments throughout the simulations. In addition, the backbone amides of the four N-terminal residues made H-bonds with the lipid phosphate groups. As shown in Figure 8 (left), the pre-A

Table 2. Tunnels Opening Frequencies (%) and Average Lengths According to the Membrane Compositions (Classical Lipid Representation) and in Solution

		DOPC	TOCL	TOCL/DOPE	solution
ST	frequency (%)	17.1 ± 1.3	25.3 ± 2.2	15.4 ± 2.0	26.5 ± 3.8
	length (Å)	14.6 ± 3.3	13.5 ± 2.2	13.9 ± 2.1	15.6 ± 2.4
LT	frequency (%)	17.2 ± 4.9	10.7 ± 1.5	17.8 ± 4.5	32.6 ± 4.5
	length (Å)	22.1 ± 3.3	22.9 ± 3.1	21.9 ± 2.2	24.1 ± 2.6
EH	frequency (%)	29.0 ± 3.4	27.2 ± 2.3	28.2 ± 3.8	22.8 ± 1.9
	length (Å)	18.4 ± 3.4	16.9 ± 2.6	16.4 ± 2.2	18.5 ± 3.4
BE	frequency (%)	5.9 ± 0.8	4.3 ± 0.5	3.1 ± 0.7	8.9 ± 1.9
	length (Å)	11.4 ± 2.1	11.6 ± 2.2	11.0 ± 1.9	12.6 ± 2.1

partitionned at the interface, at the average lipid phosphate group level along the bilayer normal, with residues interacting with the polar and the nonpolar lipid groups. This interaction between the lipids and the pre-A helix resulted in a reorientation of the pre-A relative to the rest of the protein, and this reorientation is slightly different according to the membrane composition, as depicted in Figure 8 (right).

Overall, the protein−lipid interactions are similar between the three lipid compositions, with two exceptions: the residues 97−108 had more interactions with DOPC bilayers, while the five last residues at the C-terminus had more interactions with TOCL-containing bilayers (Figure 7). Interestingly, the negatively charged residue Asp100, located on the G helix, was exposed to the bilayer. The electrostatic potential of the pre-A, B, and G helices is represented in Figure S15.

Modulation of Access Tunnels. From the simulations, the positioning of HbN on membranes leads to configurations for which the ST was oriented toward the inside of the membrane, for the three membrane compositions (Figure 6). All the other tunnel entrances observed in HbN were facing the bulk solvent. We have calculated the tunnel formation frequencies and lengths according to membrane compositions, and the results are presented in Table 2. The statistics are also presented for HbN in solution, for comparison. In all cases, the four tunnels observed in solution were also present when HbN was bound to membranes. The lengths of the tunnels were similar in all cases. However, the frequencies of opening events differed according to the systems: the LT was the most often open in solution, while it was the EH tunnel in the presence of membranes. The opening of the LT was significantly less frequent for HbN bound to membranes. The frequencies of the ST opening in solution and in the presence of pure TOCL were similar and elevated, while the opening events of ST were significantly lower in the presence of DOPC and TOCL/DOPE membranes. When taking all the tunnels opening statistics together, the frequencies of tunnel opening were higher in solution than in the presence of membranes. However, this result does not imply lower rates of ligand entry in the presence of membranes, as the presence of the ligand at the entry can catalyze the opening of the tunnels.[36]

■ DISCUSSION

The goal of this study was to determine the interactions between HbN and model membranes, and thus provide a molecular model that would bring insights on the mechanism of ligand capture from the membrane. To achieve this goal, we have used a combination of spectroscopic and molecular modeling techniques. The study was realized using three membrane compositions: pure DOPC, pure TOCL, and a mix of TOCL/DOPE at a molar ratio of 3:1. These lipids were chosen as the CL and PE phospholipids are major structural components of the mycobacterial plasma membrane and PC phospholipids are absent from the mycobacterium plasma membranes,[40] but the principal constituent of the extracellular leaflet of mammalian cell membranes.[41]

The results included in the present work clearly demonstrated that HbN binds at the surface of biological membranes. Both NMR and FTIR spectrocopy highlighted the protein−lipid interactions that occur upon HbN binding to the membranes, and the results were corroborated by the molecular modeling results. Moreover, the circular dichroism results indicated that the secondary structure of the protein was the same for the protein in solution and in the presence of lipids, which is also in agreement with the simulation results. This confirms the hypothesis that HbN is an amphitropic protein,[74] i.e., a protein that exists both in solution and associated with lipid membranes while maintaining the same secondary structure.

From molecular modeling, the relative times of contact between HbN residues and the membranes (Figure 7) indicated that the binding of HbN to the membranes occurred via the pre-A, G, and H helices for all three membrane compositions. The resulting protein orientation and insertion in membranes observed in the present work are in good agreement with the prediction of the PPM server,[39] as shown in Figure S1, but disagree with the MPEx[38] prediction. In contrast to MPEx, the PPM server uses the 3D protein structures and, in addition to the hydrophobic interactions, accounts for the hydrogen bonding and electrostatic interactions of the proteins with an anisotropic water−lipid environment. Further, other membrane prediction tools, such as TMHMM 2.0[75] and TOPCONS,[76] did not predict HbN as a membrane protein. The agreement with only the PPM server is an indication that the electrostatic interactions and the 3D structure, which are not used by the other prediction methods, are playing a key role in the binding of HbN to the membranes.

Although the membrane positioning of HbN observed from molecular modeling was similar for the three membrane compositions used in this study, small differences were observed according to the nature of the lipids present in the membranes. The solid-state ^{31}P NMR results showed that HbN induced a small proportion of hexagonal II phase in certain lipids such as DOPC but maintained the integrity of membranes when associated with TOCL and TOCL/DOPE. This is in agreement with simulation results that indicated that the protein interacted more with lipids in DOPC membranes than in TOCL-containing membranes, most likely due to the absence of a net negative charge in these membranes. The molecular modeling results suggest that Asp100 is responsible for the differences in binding of HbN according to the

electrostatic potential of the membrane. This conclusion also suggests that the binding of HbN to membranes would vary according to the salt concentration of the solution. The introduction of small negative curvature constraints in the DOPC membranes by HbN might be responsible for the formation of a small proportion of hexagonal II phase at the lipid/protein ratio of 60:1 used in the present study. However, this phenomenon might not be observed at a lower protein concentration. It can also be noted that the formation of the hexagonal II phase is favored by dehydration of the lipid polar headgroups.[77] This is in agreement with the higher wavenumber obtained for the C=O stretching vibration observed for DOPC lipid vesicles in the presence of HbN.

Significant interactions between HbN and the membranes arose from the pre-A helix (Figures 7 and 8 (left)). This segment of the protein is composed of a mix of polar and nonpolar amino acids, giving rise to interactions with both the lipids polar heads and the aliphatic chains, leading to a positioning at the membrane interface. It is noteworthy that the two arginines were in contact with both the polar heads and the aliphatic chains throughout the simulations for all three membrane compositions. No other amino acids in the HbN sequence interacted more with the membrane than these two arginines. The association of HbN with the membranes also occurred via the G and H helices, which is in agreement with the membrane localization of the pre-A-deleted HbN observed experimentally.[18] This last interaction was modulated by the electrostatic interactions between the lipid membranes and the Asp100 residue from the G helix. Therefore, HbN would be allowed to modulate the binding to the membranes according to their lipid composition. It is interesting to note that the pre-A, G, and H helices are conserved among HbN from few other Mycobacteria (see Figure S16).

For all three membrane compositions used in this study, the analysis of the CH_2 symmetric stretching vibration by infrared spectroscopy showed that HbN had very little effect on the lipid acyl chains. This is again in agreement with the fact that HbN would be located at the interface of the lipid bilayers. Our results therefore indicate that HbN is an amphitropic protein, located at the interface of lipid bilayers. Moreover, the membranes exerted a limited influence on the dynamics of HbN, as noted by small differences in frequencies of tunnel formation for HbN bound to membranes. The positioning of HbN on the membranes as observed in this work leads to the exposition of the ST entrance oriented toward the membrane, while the other tunnel entrances were oriented toward the bulk solvent. This orientation was to be expected as the ST entrance covers a large hydrophobic funnel-shape area extending far from the tunnel entrance. As the ST is preferentially used by small apolar ligands to reach the distal heme pocket,[36] it is expected to play a similar role when bound to membranes. It is interesting to note that nitric oxide is three times more soluble in lipid membranes than in an aqueous buffer, while the opposite is observed for nitrate.[17] The interfacial location of HbN would greatly facilitate the recruitment of NO, and NO_3^- to exit more easily through solvent-accessible tunnels. A similar interfacial binding was also reported for the human cytochrome P450, for which the membrane binding does not alter significantly the flexibility of the protein[32] but results in conformational changes that facilitate the ligand access to the tunnels leading to the active site of the enzyme.[33]

A recent study has revealed an O-mannosylation site at the C-terminal region of HbN that is post-translationally modified

by glycan linkage in Mtb.[18] The glycosylation site is located at residues T132 and T133, in the unstructured and flexible region following the C-terminal end of the membrane-bound H helix. According to our results (Figures 6 and 7), these amino acids are located at the interface of the bilayer, in the lipid phosphate region. These results suggest that the addition of mannose, the glycan linker identified by Arya et al.,[18] to these residues should not alter significantly the binding of HbN to membranes. As a consequence, the mechanistic conclusions presented here should not be altered by the glycosylation of HbN. Furthermore, the glycosylation of HbN was associated with both an extracytoplasmic membrane localization and an enhanced NO uptake when expressed in *Mycobacterium smegmatis*.[18] This increase in NO uptake might arise from a localization closer to the external NO source, which would be catched when reaching the membrane, and would also favor the exit of nitrate outside of bacterial cell. In addition, Singh at al. investigated the enzymatic reduction of Mtb HbN by the *E. coli* NADH-flavodoxin reductase (FdR).[78] They reported that the CD loop of HbN (residues D40 to F46, Figure 7) forms contacts with FdR. Also, the pre-A segment is involved in the heme iron reduction by FdR indirectly from its large flexibility that allows transient electrostatic contacts with the protein core that influence significantly the motion of the protein backbone. According to our membrane-bound HbN model (Figure 6), the CD loop is completely exposed to the solvent, and the interaction with another protein is then possible. On the other hand, the dynamics of the pre-A segment and the protein core is profoundly modified following the binding at the membrane interface (Figure 8), as it would also be the case for the dynamics of the complete protein. However, as the change in the dynamics of HbN upon membrane binding has not been determined in this study, we cannot assess this impact on the interaction between HbN and FdR.

■ ASSOCIATED CONTENT

Ⓢ Supporting Information

A comparison of the typical HbN orientation from MD simulations using the classical lipid representation and the membrane binding prediction of HbN from the PPM server; the initial protein orientations and final snapshots of HbN at the DCLE—water interface; the infrared and second derivative spectra; the HbN center of mass, orientation and RMSD time series for the different lipid representations; the HbN secondary structure from the simulations and the electrostatic potential on HbN surface. This material is available free of charge via the Internet at http://pubs.acs.org.

■ AUTHOR INFORMATION

Corresponding Author

*E-mail: Patrick.Lague@bcm.ulaval.ca.

■ ABBREVIATIONS

2/2Hbs; 2-on-2 hemoglobins; CD; circular dichroism; CSA; chemical shift anisotropy; DCLE; 1,1-dichloroethane; DOPC; dioleoylphosphatidylcholine; DOPE; dioleoylphosphatidylethanolamine; DVPC; divalerylphosphatidylcholine; DVPE; divalerylphosphatidylethanolamine; FTIR; Fourier transform infrared; HMMM; highly mobile membrane-mimetic; LT; long tunnel; MD; molecular dynamics; NOD; nitric oxide dioxygenase reaction; NMR; nuclear magnetic resonance; ST; short tunnel; TOCL; tetraoleoyl cardiolipin; TVCL; tetravaleryl cardiolipin

■ REFERENCES

(1) Wittenberg, J. B., Bolognesi, M., Wittenberg, B. A., and Guertin, M. (2002) Truncated hemoglobins: A new family of hemoglobins widely distributed in bacteria, unicellular eukaryotes, and plants. *J. Biol. Chem. 277*, 871−874.

(2) Vuletich, D., and Lecomte, T. (2006) A phylogenetic and structural analysis of truncated hemoglobins. *J. Mol. Evol. 62*, 196−210.

(3) Nardini, M., Pesce, A., Milani, M., and Bolognesi, M. (2007) Protein fold and structure in the truncated (2/2) globin family. *Gene 398*, 2−11.

(4) Vinogradov, S. N., Tinajero-Trejo, M., Poole, R. K., and Hoogewijs, D. (2013) Bacterial and archaeal globins - A revised perspective. *Biochim. Biophys. Acta 1834*, 1789−1800.

(5) Pesce, A., Bolognesi, M., Nardini, M. (2013) *Advances in Microbial Physiology* (Poole, R. K., Ed.) Vol. 63, pp 49−78, Academic Press LTD - Elsevier Science LTD, London.

(6) Ouellet, H., Ouellet, Y., Richard, C., Labarre, M., Wittenberg, B., Wittenberg, J., and Guertin, M. (2002) Truncated hemoglobin HbN protects *Mycobacterium bovis* from nitric oxide. *Proc. Natl. Acad. Sci. U.S.A 99*, 5902−5907.

(7) Dikshit, R. P., Dikshit, K. L., Liu, Y. X., and Webster, D. A. (1992) The bacterial hemoglobin from Vitreoscilla can support the aerobic growth of *Escherichia coli* lacking terminal oxidases. *Arch. Biochem. Biophys. 293*, 241−245.

(8) Wainwright, L. M., Elvers, K. T., Park, S. F., and Poole, R. K. (2005) A truncated haemoglobin implicated in oxygen metabolism by the microaerophilic food-borne pathogen *Campylobacter jejuni*. *Microbiology 151*, 4079−4091.

(9) Pathania, R., Navani, N., Rajomohan, G., and Dikshit, K. (2002) *Mycobacterium tuberculosis* hemoglobin HbO associates with membranes and stimulates cellular respiration of recombinant *Escherichia coli*. *J. Biol. Chem. 277*, 15293−15302.

(10) Liu, C., He, Y., and Chang, Z. (2004) Truncated hemoglobin O of *Mycobacterium tuberculosis*: the oligomeric state change and the interaction with membrane components. *Biochem. Biophys. Res. Commun. 316*, 1163−1172.

(11) Daigle, R., Guertin, M., and Lagüe, P. (2009) Structural characterization of the tunnels of *Mycobacterium tuberculosis* truncated hemoglobin N from molecular dynamics simulations. *Proteins 75*, 735−747.

(12) Pesce, A., Couture, M., Dewilde, S., Guertin, M., Yamauchi, K., Ascenzi, P., Moens, L., and Bolognesi, M. (2000) A novel two-over-two alpha-helical sandwich fold is characteristic of the truncated hemoglobin family. *EMBO J. 19*, 2424−2434.

(13) Milani, M., Pesce, A., Ouellet, Y., Ascenzi, P., Guertin, M., and Bolognesi, M. (2001) Mycobacterium tuberculosis hemoglobin N displays a protein tunnel suited for O2 diffusion to the heme. *EMBO. J. 20*, 3902−3909.

(14) Oliveira, A., Singh, S., Bidon-Chanal, A., Forti, F., Martì, M. A., Boechi, L., Estrin, D. A., Dikshit, K. L., and Luque, F. J. (2012) Role of PheE15 gate in ligand entry and nitric oxide detoxification function of *Mycobacterium tuberculosis* truncated hemoglobin N. *PLoS One 7*, e49291.

(15) Dzikovski, B. G., Livshits, V. A., and Marsh, D. (2003) Oxygen permeation profile in lipid membranes: comparison with transmembrane polarity profile. *Biophys. J. 85*, 1005−1012.

(16) Wang, Y., Cohen, J., Boron, W. F., Schulten, K., and Tajkhorshid, E. (2007) Exploring gas permeability of cellular membranes and membrane channels with molecular dynamics. *J. Struct. Biol. 157*, 534−544.

(17) Möller, M. N., Jr. Lancaster, J. R., Denicola, A. (2008) Current Topics in Membranes, in *Free Radical Effects on Membranes* (Matalon, S., Ed.) Vol. 61, pp 23−42, Academic Press, New York.

(18) Arya, S., Sethi, D., Singh, S., Hade, M. D., Singh, V., Raju, P., Chodisetti, S. B., Verma, D., Varshney, G. C., Agrewala, J. N., et al. (2013) Truncated Hemoglobin, HbN, Is Post-translationally Modified in *Mycobacterium tuberculosis* and Modulates Host-Pathogen Interactions during Intracellular Infection. *J. Biol. Chem. 288*, 29987−29999.

(19) Couture, M., Chamberland, H., St-Pierre, B., Lafontaine, J., and Guertin, M. (1994) Nuclear genes encoding chloroplast hemoglobins in the unicellular green alga Chlamydomonas eugametos. *Mol. Gen. Genet. 243*, 185−197.

(20) Hill, D. R., Belbin, T. J., Thorsteinsson, M. V., Bassam, D., Brass, S., Ernst, A., Böger, P., Paerl, H., Mulligan, M. E., and Potts, M. (1996) GlbN (cyanoglobin) is a peripheral membrane protein that is restricted to certain Nostoc spp. *J. Bacteriol. 178*, 6587−6598.

(21) Gardner, P. R. (2012) Hemoglobin: A Nitric-Oxide Dioxygenase. *Scientifica 2012*, 1−34.

(22) Ramandeep, Hwang, K. W., Raje, M., Kim, K. J., Stark, B. C., Dikshit, K. L., and Webster, D. A. (2001) Vitreoscilla hemoglobin. Intracellular localization and binding to membranes. *J. Biol. Chem. 276*, 24781−24789.

(23) Rinaldi, A. C., Bonamore, A., Macone, A., Boffi, A., Bozzi, A., and Di Giulio, A. (2006) Interaction of Vitreoscilla Hemoglobin with Membrane Lipids. *Biochemistry 45*, 4069−4076.

(24) Di Giulio, A., and Bonamore, A. (2008) Globin Interactions with Lipids and Membranes. *Methods Enzymol.*, 239−253.

(25) Ertas, B., Kiger, L., Blank, M., Marden, M. C., and Burmester, T. (2011) A membrane-bound hemoglobin from gills of the green shore crab Carcinus maenas. *J. Biol. Chem. 286*, 3185−3193.

(26) Blank, M., Wollberg, J., Gerlach, F., Reimann, K., Roesner, A., Hankeln, T., Fago, A., Weber, R. E., and Burmester, T. (2011) A membrane-bound vertebrate globin. *PLoS One 6*, e25292.

(27) Cassanova, N., O'Brien, K. M., Stahl, B. T., McClure, T., and Poyton, R. O. (2005) Yeast flavohemoglobin, a nitric oxide oxidoreductase, is located in both the cytosol and the mitochondrial matrix: effects of respiration, anoxia, and the mitochondrial genome on its intracellular level and distribution. *J. Biol. Chem. 280*, 7645−7653.

(28) Kim, D. Y., Hong, M. J., Lee, Y. J., Lee, M. B., and Seo, Y. W. (2012) Wheat truncated hemoglobin interacts with photosystem I PSK-I subunit and photosystem II subunit PsbS1. *Biol. Plant 57*, 281−290.

(29) Bonamore, A., Farina, A., Gattoni, M., Schininà, M. E., Bellelli, A., and Boffi, A. (2003) Interaction with membrane lipids and heme ligand binding properties of *Escherichia coli* flavohemoglobin. *Biochemistry 42*, 5792−5801.

(30) Ermler, U., Siddiqui, R. A., Cramm, R., and Friedrich, B. (1995) Crystal structure of the flavohemoglobin from Alcaligenes eutrophus at 1.75 Å resolution. *EMBO J. 14*, 6067−6077.

(31) Ollesch, G., Kaunzinger, A., Juchelka, D., Schubert-Zsilavecz, M., and Ermler, U. (1999) Phospholipid bound to the flavohemoprotein from Alcaligenes eutrophus. *Eur. J. Biochem. 262*, 396−405.

(32) Cojocaru, V., Balali-Mood, K., Sansom, M. S. P., and Wade, R. C. (2011) Structure and dynamics of the membrane-bound Cytochrome P450 2C9. *PLoS Comput. Biol. 7*, e1002152.

(33) Baylon, J. L., Lenov, I. L., Sligar, S. G., and Tajkhorshid, E. (2013) Characterizing the membrane-bound state of Cytochrome P450 3A4: Structure, depth of insertion, and orientation. *J. Am. Chem. Soc. 135*, 8542−8551.

(34) Berka, K., Paloncỳovà, M., Anzenbacher, P., and Otyepka, M. (2013) Behavior of human cytochromes P450 on lipid membranes. *J. Phys. Chem. B 117*, 11556−11564.

(35) Via, L. E., et al. (2008) Tuberculous granulomas are hypoxic in guinea pigs, rabbits, and nonhuman primates. *Infect. Immun. 76*, 2333−2340.

(36) Daigle, R., Rousseau, J.-A., Guertin, M., and Lagüe, P. (2009) Theoretical investigations of nitric oxide channeling in *Mycobacterium tuberculosis* truncated hemoglobin N. *Biophys. J. 97*, 2967−2977.

(37) MÅlen, H., Pathak, S., Søfteland, T., de Souza, G. A., and Wiker, H. G. (2010) Definition of novel cell envelope associated proteins in Triton X-114 extracts of Mycobacterium tuberculosis H37Rv. *BMC. Microbiol. 10*, 132−143.

(38) Snider, C., Jayasinghe, S., Hristova, K., and White, S. H. (2009) MPEx: a tool for exploring membrane proteins. *Protein Sci. 18*, 2624−2628.

(39) Lomize, M. A., Pogozheva, I. D., Joo, H., Mosberg, H. I., and Lomize, A. L. (2012) OPM database and PPM web server: resources for positioning of proteins in membranes. *Nucleic Acids Res. 40*, D370−D376.

(40) Sareen, M., and Khuller, G. K. (1990) Cell wall and membrane changes associated with ethambutol resistance in *Mycobacterium tuberculosis* H37Ra. *Antimicrob. Agents Chemother. 34*, 1773−1776.

(41) Kiessling, V., Wan, C., and Tamm, L. K. (2009) Domain coupling in asymmetric lipid bilayers. *Biochim. Biophys. Acta 1788*, 64−71.

(42) Savard, P.-Y., Daigle, R., Morin, S., Sebilo, A., Meindre, F., Lagüe, P., Guertin, M., and Gagné, S. M. (2011) Structure and dynamics of *Mycobacterium tuberculosis* truncated hemoglobin N: Insights from NMR spectroscopy and molecular dynamics simulations. *Biochemistry 50*, 11121−11130.

(43) Rance, M., and Byrd, R. (1983) Obtaining high-fidelity spin-1/2 powder spectra in anisotropic media - phased-cycled Hahn echo spectroscopy. *J. Magn. Reson. 52*, 221−240.

(44) Phillips, J. C., Braun, R., Wang, W. E. I., Gumbart, J., Tajkhorshid, E., Villa, E., Chipot, C., Skeel, R. D., Schulten, K., and Kale, L. (2005) Scalable molecular dynamics with NAMD. *J. Comput. Chem. 26*, 1781−1802.

(45) MacKerell, A., and Bashford, D. (1998) All-atom empirical potential for molecular modeling and dynamics studies of proteins. *J. Phys. Chem. B 5647*, 3586−3616.

(46) Mackerell, A. D., Feig, M., and Brooks, C. L. (2004) Extending the treatment of backbone energetics in protein force fields: limitations of gas-phase quantum mechanics in reproducing protein conformational distributions in molecular dynamics simulations. *J. Comput. Chem. 25*, 1400−1415.

(47) Klauda, J. B., Venable, R. M., Freites, J. A., O'Connor, J. W., Tobias, D. J., Mondragon-Ramirez, C., Vorobyov, I., MacKerell, A. D., Jr., and Pastor, R. W. (2010) Update of the CHARMM all-atom additive force field for lipids: validation on six lipid types. *J. Phys. Chem. B 114*, 7830−7843.

(48) Jorgensen, W. L., Chandrasekhar, J., Madura, J. D., Impey, R. W., and Klein, M. L. (1983) Comparison of simple potential functions for simulating liquid water. *J. Chem. Phys. 79*, 926−935.

(49) Durell, S. R., Brooks, B. R., and Ben-Naim, A. (1994) Solvent-induced forces between two hydrophilic groups. *J. Chem. Phys.*, 2198−2202.

(50) Darden, T., York, D., and Pedersen, L. G. (1993) Particle mesh Ewald: An Nlog(N) method for Ewald sums in large systems. *J. Chem. Phys. 98*, 10089−10092.

(51) Essmann, U., Perera, L., Berkowitz, M. L., Darden, T., Lee, H., and Pedersen, L. G. (1995) A smooth particle mesh Ewald method. *J. Chem. Phys. 103*, 8577−8593.

(52) Brooks, B. R., Brooks, C. L., III, Mackerell, A. D., Nilsson, L., Petrella, R. J., Roux, B., Won, Y., Archontis, G., Bartels, C., Boresch, S., Caflisch, A., Caves, L., Cui, Q., Dinner, A. R., and Feig, M. (2009) CHARMM: the biomolecular simulation program. *J. Comput. Chem. 30*, 1545−1614.

(53) Humphrey, W., Dalke, A., and Schulten, K. (1996) VMD: visual molecular dynamics. *J. Mol. Graph. 14*, 33−38.

(54) Arcario, M. J., Ohkubo, Y. Z., and Tajkhorshid, E. (2011) Capturing spontaneous partitioning of peripheral proteins using a biphasic membrane-mimetic model. *J. Phys. Chem. B 115*, 7029−7037.

(55) Vanommeslaeghe, K., Hatcher, E., Acharya, C., Kundu, S., Zhong, S., Shim, J., Darian, E., Guvench, O., Lopes, P., Vorobyov, I., and Mackerell, A., Jr. (2010) CHARMM general force field: A force field for drug-like molecules compatible with the CHARMM all-atom additive biological force fields. *J. Comput. Chem. 31*, 671−690.

(56) Yu, W., He, X., Vanommeslaeghe, K., and MacKerell, A. D. (2012) Extension of the CHARMM general force field to sulfonyl-containing compounds and its utility in biomolecular simulations. *J. Comput. Chem. 33*, 2451−2468.

(57) Ohkubo, Y., Pogorelov, T., Arcario, M., Christensen, G., and Tajkhorshid, E. (2012) Accelerating membrane insertion of peripheral proteins with a novel membrane mimetic model. *Biophys. J. 102*, 2130−2139.

(58) Woolf, T. B., and Roux, B. (1996) Structure, energetics, and dynamics of lipid-protein interactions: A molecular dynamics study of the gramicidin A channel in a DMPC bilayer. *Proteins 24*, 92−114.

(59) Jo, S., Kim, T., and Im, W. (2007) Automated builder and database of protein/membrane complexes for molecular dynamics simulations. *PloS. ONE 2*, e880.

(60) Jo, S., Lim, J. B., Klauda, J. B., and Im, W. (2009) CHARMM-GUI Membrane Builder for mixed bilayers and its application to yeast membranes. *Biophys. J. 97*, 50−58.

(61) Kucerka, N., Nagle, J. F., Sachs, J. N., Feller, S. E., Pencer, J., Jackson, A., and Katsaras, J. (2008) Lipid bilayer structure determined by the simultaneous analysis of neutron and X-ray scattering data. *Biophys. J. 95*, 2356−2367.

(62) Aguayo, D., González-Nilo, F. D., and Chipot, C. (2012) Insight into the Properties of Cardiolipin Containing Bilayers from Molecular Dynamics Simulations, Using a Hybrid All-Atom/United-Atom Force Field. *J. Chem. Theory Comput. 8*, 1765−1773.

(63) Rand, R., and Parsegian, V. (1989) Hydration forces between phospholipid bilayers. *Biochim. Biophys. Acta 988*, 351−376.

(64) Chovancova, E., Pavelka, A., Benes, P., Strnad, O., Brezovsky, J., Kozlikova, B., Gora, A., Sustr, V., Klvana, M., Medek, P., Biedermannova, L., Sochor, J., and Damborsky, J. (2012) CAVER 3.0: a tool for the analysis of transport pathways in dynamic protein structures. *PLoS Comput. Biol. 8*, e1002708.

(65) Johnson, W., Jr. (1990) Protein secondary structure and circular dichroism: a practical guide. *Proteins 7*, 205−214.

(66) Seelig, J. (1978) P_{31} nuclear magnetic-resonance and head group structure of phospholipids in membranes. *Biochim. Biophys. Acta 515*, 105−140.

(67) Seelig, J., and Seelig, A. (1980) Lipid conformation in model membranes and biological membranes. *Q. Rev. Biophys. 13*, 19−61.

(68) Smith, I. C. P., Ekiel, I. H. (1984) Phosphorus-31 NMR of phospholipids in membranes, in *Phosphorous-31 NMR: Principles and Applications*, Academic Press, New-York.

(69) Henderson, T. O., Glonek, T., and Myers, T. C. (1974) Phosphorus-31 nuclear magnetic resonance spectroscopy of phospholipids. *Biochemistry 13*, 623−628.

(70) Picard, F., Paquet, M. J., Levesque, J., Bélanger, A., and Auger, M. (1999) ^{31}P NMR first spectral moment study of the partial

magnetic orientation of phospholipid membranes. *Biophys. J. 77*, 888−902.

(71) Mantsch, H. H., and McElhaney, R. N. (1991) Phospholipid phase transitions in model and biological membranes as studied by infrared spectroscopy. *Chem. Phys. Lipids 57*, 213−226.

(72) Lewis, R. N., McElhaney, R. N., Pohle, W., and Mantsch, H. H. (1994) Components of the carbonyl stretching band in the infrared spectra of hydrated 1,2-diacylglycerolipid bilayers: a reevaluation. *Biophys. J. 67*, 2367−2375.

(73) Blume, A., Hübner, W., and Messner, G. (1988) Fourier transform infrared spectroscopy of ^{13}C=O-labeled phospholipids hydrogen bonding to carbonyl groups. *Biochemistry 27*, 8239−8249.

(74) Johnson, J., and Cornell, R. (1999) Amphitropic proteins: regulation by reversible membrane interactions (review). *Mol. Membr. Biol. 16*, 217−235.

(75) Krogh, A., Larsson, B., von Heijne, G., and Sonnhammer, E. L. (2001) Predicting transmembrane protein topology with a hidden Markov model: application to complete genomes. *J. Mol. Biol. 305*, 567−580.

(76) Bernsel, A., Viklund, H., Hennerdal, A., and Elofsson, A. (2009) TOPCONS: consensus prediction of membrane protein topology. *Nucleic Acids Res. 37*, W465−W468.

(77) Powell, G. L., and Marsh, D. (1985) Polymorphic phase behavior of cardiolipin derivatives studied by ^{31}P NMR and X-ray diffraction. *Biochemistry 24*, 2902−2908.

(78) Singh, S., Thakur, N., Oliveira, A., Petruk, A. A., Hade, M. D., Sethi, D., Bidon-Chanal, A., Marti, M. A., Datta, H., Parkesh, R., et al. (2014) Mechanistic insight into the enzymatic reduction of truncated hemoglobin N of *Mycobacterium tuberculosis*: role of the CD loop and pre-A motif in electron cycling. *J. Biol. Chem. 289*, 21573−21583.